ACS AuthorChoice

ARTICLE

Bottlebrush Block Polymers: Quantitative Theory and Experiments

Samuel J. Dalsin,[†] Thomas G. Rions-Maehren,[‡] Marissa D. Beam,[†] Frank S. Bates,[*,†] Marc A. Hillmyer,[*,‡] and Mark W. Matsen[*,§]

[†]Department of Chemical Engineering and Materials Science and [‡]Department of Chemistry, University of Minnesota, Minneapolis, Minnesota 55455-0431, United States and [§]Department of Chemical Engineering, Department of Physics & Astronomy, Waterloo Institute for Nanotechnology, University of Waterloo, Waterloo, Ontario N2L 3G1, Canada

ABSTRACT The self-assembly of bottlebrush block polymers into a lamellar phase was investigated using a combination of experiment and self-consistent field theory (SCFT). Nine diblock bottlebrush polymers were synthesized with atactic polypropylene side chains (block A) and polystyrene side chains (block B) attached to poly(norbornene) backbones of various contour lengths, L, and the resulting lamellar structures were analyzed using small-angle X-ray scattering. The scaling of the lamellar period, $d_0 \sim L^{\gamma}$, exhibited an increasing exponent from $\gamma \approx 0.3$ at small L to $\gamma \approx 0.9$ at large L. The small exponents occurred for starlike molecules where the size of the side chains is comparable to L, while the larger exponents occurred for the more brushlike molecules where the side chains extend radially outward from the backbone. The bottlebrushes were then modeled using flexible side chains of types A and B attached to a semiflexible backbone with an adjustable persistence length, ξ_b. The resulting SCFT predictions for d_0 showed remarkable quantitative agreement with the experimental data, where ξ_b was similar to the radius of the bottlebrushes. The theory was then used to examine the joint-distribution functions for the position and orientation of different segments along the backbone. This revealed a bilayer arrangement of the bottlebrushes in the lamellar phase, with a high degree of backbone orientation at the A/B interfaces that almost completely vanished near the center of the domains. This finding clearly refutes the prevailing interpretation that the large scaling exponent γ is a result of highly extended backbone conformations.

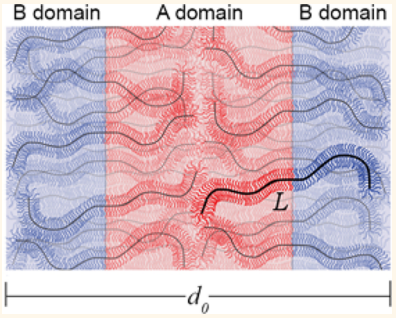

KEYWORDS: bottlebrush · self-assembly · lamellae · block copolymer · self-consistent field theory

Bottlebrush polymers represent a new class of macromolecules that have become an exciting and active area of research in polymer science and engineering. Consisting of densely spaced side chains grafted along a central backbone, bottlebrush polymers are typically of ultrahigh molar mass and display extended wormlike conformations.[1−5] These characteristic properties cause bottlebrush polymers to exhibit distinctive behavior compared to their linear counterparts, and make them attractive candidates for creating advanced materials with potential applications in lithography,[6] photonic crystals,[7−10] and surface coatings.[11] Due to the many independent molecular parameters, a myriad of bottlebrush copolymer architectures can be designed by incorporating two or more different chemical repeat units. For instance, block and random copolymer brushes have been prepared by regulating the arrangement of chemically distinct side chains along the backbone.[9,12] Alternatively, multicomponent structures such as core−shell cylinders can be synthesized by using block polymer side chains.[12−17] These molecules can be further tailored for specific applications by, for example, including chemically degradable blocks or by decorating side chains with a desired functionality.[6,13,16,17] To fully exploit the countless possibilities and enable controlled design of nanostructured materials from bottlebrush polymers, a more complete fundamental understanding of the self-assembly behavior is needed. With this in mind, we focus here on the simplest case, that is, diblock bottlebrush self-assembly into the lamellar phase.

Prior experimental studies have demonstrated that diblock polymers with at least one bottlebrush block readily self-assemble into ordered morphologies with domain sizes much larger than can be attained using linear block polymers.[9,18,19] The kinetics of bottlebrush ordering is much faster

* Address correspondence to bates001@umn.edu, hillmyer@umn.edu, mwmatsen@uwaterloo.ca.

Received for review August 31, 2015 and accepted October 27, 2015.

Published online November 06, 2015
10.1021/acsnano.5b05473

than that of linear diblocks large enough to produce similar-sized domains. This is because the high entanglement density that hinders ordering in high molar mass linear polymer melts is generally absent in bottlebrush systems due to the large macromolecular cross-sectional area. Studies have also shown that densely branched bottlebrush diblocks have a strong tendency to form lamellar morphologies, even for systems with highly asymmetric volume fractions. This has been attributed to the semirigid molecular structure, which favors the flat domain interfaces afforded by the lamellar phase.[20] However, Bolton et al. demonstrated that diblocks with significant asymmetry in side chain lengths could self-assemble into cylindrical morphologies.[21] In this case, the cylindrical phase is stabilized by the architectural asymmetry of bottlebrushes with long branches on one half of the backbone and short branches on the other half. More recently, Gu et al. reported the synthesis of several symmetric bottlebrush diblocks with independently varied side chain and backbone lengths.[22] This study utilized precisely defined bottlebrush polymers to examine the self-assembly kinetics and domain spacing achieved in the ordered structures.

The molecular complexity of bottlebrush molecules poses an immense challenge in understanding and predicting structural and dynamic behaviors. Bottlebrush diblocks involve far more molecular parameters than linear diblocks, the effects of which are difficult to resolve. One approach to studying the effects of the different parameters is through simulation. This is not so practical, however, because of the computational demands of simulating such large molecules. As an example, Chremos and Theodorakis recently examined the assembly of bottlebrush block polymers by molecular dynamics simulations of a simple bead−spring model.[23] This method yielded morphology diagrams of polymers with various degrees of architectural asymmetry, but was limited to a small number of beads per molecule. Consequently, either the branches were very short (often just one bead) or the number of branches was very small (as few as one A-type or one B-type branch). Gu et al. performed simulations similar to those of Chremos and Theodorakis, but with degrees of polymerization that were more representative of real bottlebrush polymers.[22] However, it does not appear that finite-size effects were addressed, given that some of the simulation boxes were barely larger than a single lamellar period. Consequently, their predictions for the scaling of lamellar domain sizes are questionable.

Adaptation of standard block polymer theories to these complex molecules is also a nontrivial task. The difficulty is that the usual mean-field approximation cannot explicitly handle the strong excluded-volume effects that exist in bottlebrushes due to the crowding of the densely packed side chains. Gu et al. presented a calculation based on the strong-segregation theory (SST) of Semenov[24] to supplement their experimental and simulation work. This implementation of SST assumed that the backbones form cylindrical domains with large diameters relative to the width of the polymer−polymer interface and small lengths relative to the contour length of the backbone. These assumptions do not conform to the molecules we are considering, since they require that the spacing between branches is large and that the lamellar period is small relative to the contour length of the backbone.

In this work, we couple state-of-the-art methods in both theory and experiments to address these outstanding problems. A new microscopic model for diblock bottlebrush polymers is first presented, which adapts self-consistent field theory (SCFT) to account for the strong steric interactions present in bottlebrush molecules. Nine model lamellar-forming diblock bottlebrush samples, denoted P(aPP)-*b*-P(PS) and containing atactic polypropylene (aPP) and polystyrene (PS) branches, have been synthesized and probed by small-angle X-ray scattering (SAXS) to determine how the domain spacing varies with the backbone chain length. Next, the experimental results are compared with model predictions. Model parameters are matched to molecules from the experimental samples, and the corresponding lamellar periods are calculated using SCFT. Validated by quantitative agreement with our experimental results, the SCFT is then used to elucidate details of how the molecules pack in the ordered state.

RESULTS AND DISCUSSION

Theoretical Model. SCFT has an impeccable track record for modeling block copolymers as well as polymeric brushes, but the combination of the two poses a challenge. In a bottlebrush molecule, the strong steric interactions cause the side chains to stretch radially outward while producing a lateral pressure that stretches the backbone and imparts it with a bending rigidity.[25,26] The crowding also shields the backbone from intermolecular interactions. These effects could be modeled using SCFT, in an analogous way to a calculation by Fredrickson,[25] but the self-consistent fields have to be solved for a fixed backbone conformation. This is because SCFT only enforces the incompressibility of the melt within the mean-field approximation. When the backbones are permitted to fluctuate, the SCFT satisfies incompressibility by smearing the high concentrations along the backbones rather than forcing the side chains to stretch. Similarly, there is an unphysical smearing of the backbone interactions. Fortunately, there are ways of correcting these shortcomings of SCFT. The steric-induced stiffness of the backbone can be incorporated by modeling it as wormlike chain.[27] The fact that the wormlike chain has a fixed contour length also allows it to handle highly extended conformations, for which the usual

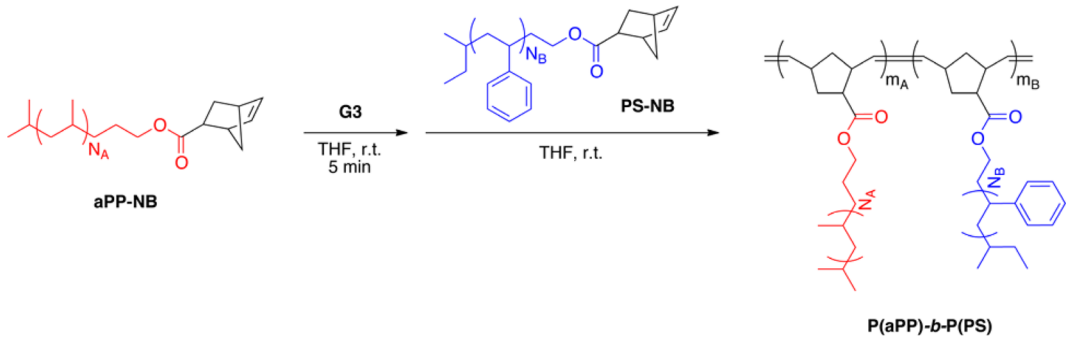

Figure 1. Synthesis of diblock bottlebrush polymers by sequential ROMP.

Gaussian-chain model would be inappropriate. Given the dense spacing of the side chains, the molecular interactions experienced by the backbone should remain relatively constant (i.e., B segments are unable to penetrate to the backbone of the A brush, and vice versa). This feature allows us to conveniently ignore all interactions involving the backbones, which solves the smearing problem. The radial stretching of the side chains is a relatively minor effect, particularly for long bottlebrushes, and so we account for this in the simplest way possible, by scaling up their segment lengths.

With these considerations in mind, we now define our model in terms of standard features.[28,29] The backbone is modeled as a wormlike chain, where its contour length, L, is fixed and its persistence length, ξ_b, is an adjustable parameter. To the backbone, we attach m_A A-type side chains of polymerization degree N_A, and m_B B-type side chains of polymerization degree N_B sequenced to form a diblock molecular architecture. The $m = m_A + m_B$ side chains are spaced uniformly along the contour of the backbone and modeled using flexible Gaussian chains with distinct statistical lengths, a_A and a_B, for the A and B segments, respectively. For simplicity, we ignore the volume of the backbone and define the A and B segments to have a common reference volume, v_{ref}, which implies that the melt is incompressible. The A/B interactions are represented using the standard Flory–Huggins parameter χ. In principle, the A and B portions of the bottlebrush would have distinct persistence lengths and different stretching factors for the side chains, but in our study the two halves of the bottlebrush are structurally similar (the spacing of the side chains is identical and the size of the A and B side chains is similar). So for simplicity, a single bending rigidity is used for the entire backbone, and the segment lengths of both A and B are scaled by the same factor.

Even with all these simplifications, our model still involves nine different parameters: L, ξ_b, χ, m_A, a_A, N_A, m_B, a_B, and N_B. In principle, we can determine them all from experiment, apart from the effective persistence length of the backbone, ξ_b, and the scaling factor for the segment lengths. The use of a scaling factor for a_A and a_B is a crude treatment of a minor effect, and so we just choose a physically reasonable value of 1.5 (i.e., we assume the crowding stretches the side chains by 50% relative to their unperturbed length). On the other hand, the behavior is very sensitive to the persistence length of the backbone and furthermore it is less clear what a reasonable value would be. Therefore, we treat ξ_b as a fitting parameter, adjusted to optimize the agreement between theory and experiment.

TABLE 1. Molecular Characterization of Norbornene-Functionalized Macromonomers

macromonomer	M_n (kg/mol)[a]	$Đ$[a]	DP[b]
aPP-NB	2.1	1.65	45
PS-NB(4.0k)	4.0	1.10	36
PS-NB(3.8k)	3.8	1.05	34

[a] Determined by SEC-MALLS in tetrahydrofuran. [b] Chemical degree of polymerization. The PS macromonomers, PS-NB(4.0k) and PS-NB(3.8k), are two different batches with comparable chain length synthesized by anionic polymerization and reversible addition–fragmentation chain transfer (RAFT) polymerization, respectively. Additional characterization is provided in the Supporting Information.

Experimental Bottlebrush Polymers. Diblock bottlebrush polymers composed of aPP side chains and PS side chains (blocks A and B, respectively) were prepared with the goal of generating lamellar morphologies and to test the theoretical predictions regarding the scaling of domain spacing as a function of backbone length. The polymer samples were synthesized by ring-opening metathesis polymerization (ROMP) of macromonomers using the Grubbs third generation catalyst [G3; $(H_2IMes)(3\text{-}BrPy)_2(Cl)_2Ru{=}CHPh$], as shown in Figure 1. ROMP of norbornene-functionalized macromonomers is an efficient method for producing bottlebrush polymers due to the high reactivity of ruthenium-based metathesis catalysts and the significant ring strain of the norbornene moiety. Furthermore, G3 has a high initiation rate, which is necessary to promote living ROMP and produce block polymers by sequential addition of macromonomers.[30–32] (See the Supporting Information for a comparison of different metathesis catalysts in these bottlebrush syntheses.)

Molecular characteristics of the aPP-NB and PS-NB macromonomers are listed in Table 1. Two batches of

TABLE 2. Molecular Characterization and Bulk Domain Spacing of Diblock Bottlebrush Polymers

sample label	$M_{n,diblock}$ (kg/mol)[a]	$Đ$[a]	ϕ_{aPP}[b]	$M_{n,aPP\text{-}NB}$ (kg/mol)	$M_{n,PS\text{-}NB}$ (kg/mol)	$DP_{aPP\text{-}NB}$[c]	$DP_{PS\text{-}NB}$[c]	d_0 (nm)[d]
[P(aPP)-*b*-P(PS)]$_{28.3k}$	28.3	1.06	0.51	2.1	4.0	6.3	3.9	16.4
[P(aPP)-*b*-P(PS)]$_{41.8k}$	41.8	1.08	0.53	2.1	3.8	10	5.7	18.3
[P(aPP)-*b*-P(PS)]$_{54.2k}$	54.2	1.05	0.51	2.1	4.0	12	7.3	21.0
[P(aPP)-*b*-P(PS)]$_{95.9k}$	95.9	1.12	0.43	2.1	3.8	18	16	26.3
[P(aPP)-*b*-P(PS)]$_{123k}$	123	1.07	0.63	2.1	3.8	35	14	32.2
[P(aPP)-*b*-P(PS)]$_{153k}$	153	1.05	0.52	2.1	4.0	35	20	38.7
[P(aPP)-*b*-P(PS)]$_{303k}$	303	1.15	0.62	2.1	3.8	84	34	73.9
[P(aPP)-*b*-P(PS)]$_{368k}$	368	1.20	0.61	2.1	4.0	100	41	81.6
[P(aPP)-*b*-P(PS)]$_{696k}$	696	1.26	0.69	2.1	4.0	219	62	149.5

[a] Determined by SEC-MALLS in tetrahydrofuran. [b] Volume fraction of aPP calculated using known densities of $\rho_{aPP} = 0.85$ g/mL and $\rho_{PS} = 1.05$ g/mL. [c] Number-average backbone degree of polymerization of each block. [d] Lamellar domain spacing calculated using the primary scattering peak ($d_0 = 2\pi/q^*$) from SAXS data at 150 °C.

PS macromonomers with similar chain lengths, PS-NB(4.0k) and PS-NB(3.8k), were prepared by anionic polymerization and reversible addition–fragmentation chain transfer (RAFT) polymerization, respectively. Consequently, the two PS-NBs have distinct end-group chemistry (characterized in the Supporting Information), and the structure of only PS-NB(4.0k) is represented in Figure 1. The P(aPP)-*b*-P(PS) bottlebrushes were synthesized by first polymerizing aPP-NB and subsequently injecting either PS-NB(3.8k) or PS-NB(4.0k) to incorporate the PS branches. While the PS branches are about twice the molar mass of the aPP branches in these bottlebrushes, the chain length of the aPP branches is slightly greater than that of the PS branches due to the lower mass per segment of aPP. Therefore, there is no significant branch length asymmetry between the two blocks. Nine diblock bottlebrush polymers of relatively symmetric brush diameter and composition ($\phi_{aPP} = 0.43–0.69$) and variable molar mass were prepared and characterized as summarized in Table 2.

Experimental Characterization Results. Samples were prepared for SAXS analysis by first solvent casting films (~1 mm thickness) from a tetrahydrofuran solution. The films were then dried under vacuum and thermally annealed at 150 °C for 4 h. [Solvent casting was used to facilitate ordering since most of the samples are of high molar mass and do not have accessible order–disorder transition temperatures (T_{ODT}).] Only [P(aPP)-*b*-P(PS)]$_{28.3k}$ had a measurable T_{ODT}, as shown in the temperature-dependent SAXS data in Figure 2. Upon heating this sample from 150 °C, the intensity of the principal peak slowly decreased, and between 210 and 220 °C the peak shape and intensity changed dramatically, indicating a transition to the disordered state. The sample was held at 220 °C for 5 min before slowly cooling. A sharp principal peak re-emerged at 215 °C and grew in intensity as it was cooled further. In contrast, all the SAXS patterns obtained from the higher molar mass P(aPP)-*b*-P(PS) specimens were consistent with states of lamellar order. Notably, [P(aPP)-*b*-P(PS)]$_{54.2k}$ did not exhibit an order–disorder transition at any temperature below the onset of thermal decomposition at 300 °C (see the Supporting Information).

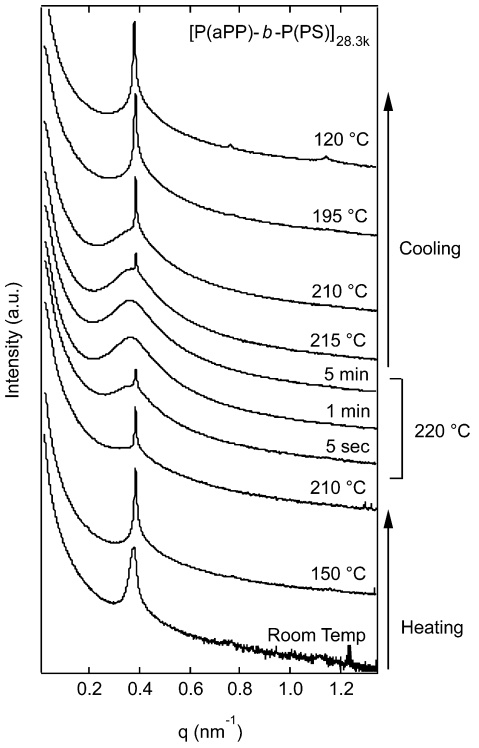

Figure 2. Temperature-dependent SAXS profiles for [P(aPP)-*b*-P(PS)]$_{28.3k}$. An order–disorder transition temperature (T_{ODT}) occurs between 215 and 220 °C.

SAXS profiles recorded at 150 °C for all of the diblock polymers are shown in Figure 3. The lamellar periodicity of each sample was calculated using $d_0 = 2\pi/q^*$, where q^* is the wavevector corresponding to the principal scattering peak. Strong reflections at integer multiples of q^* in many of the samples confirm a well-ordered lamellar morphology. A few of the samples, [P(aPP)-*b*-P(PS)]$_{95.9k}$ in particular, display low intensity peaks at scattering vectors less than q^*. We attribute these features to incomplete thermal annealing following the solvent casting procedure, which may cause kinetically trapped morphologies such as local disorder and produce a broad peak at $q < q^*$

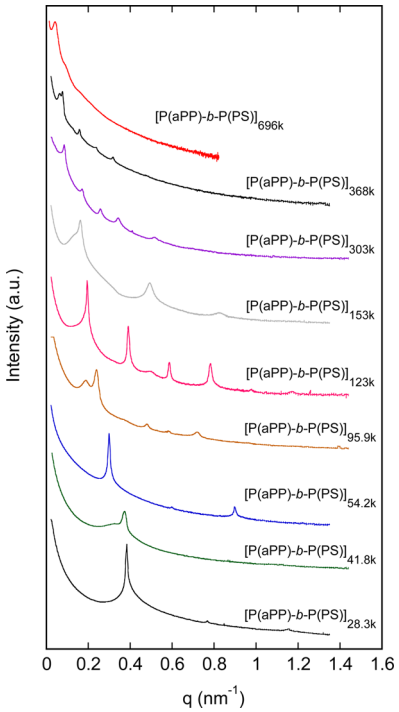

Figure 3. SAXS profiles of the undiluted diblock bottlebrush polymers at 150 °C.

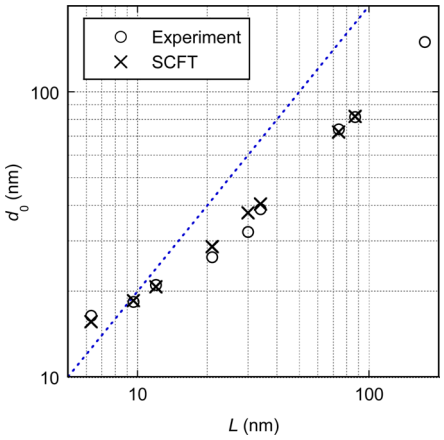

Figure 4. Lamellar periodicity, d_0, versus contour length of the backbone, L, obtained from the experimental SAXS measurements and the SCFT predictions. The blue dotted line denotes the upper limit for long bottlebrush molecules, $d_0 = 2L$, corresponding to a lamellar period consisting of two fully extended diblock monolayers.

(see Figure 2). Additionally, the well-defined scattering pattern from [P(aPP)-*b*-P(PS)]$_{123k}$ includes an anomalous feature between the second and third order Bragg reflections. There is also some evidence of this peak in the [P(aPP)-*b*-P(PS)]$_{95.9k}$ profile. We do not know the origins of this feature, but speculate that it may be caused by metastable defects in the microstructure. Nevertheless, the sharp peaks at q^* along with distinct peaks at $2q^*$ and $3q^*$ support the presence of lamellar domains in these samples. The SAXS data for the highest molar mass diblock, [P(aPP)-*b*-P(PS)]$_{696k}$, was obtained using an incident beam of lower energy (longer X-ray wavelength) than the other samples, enabling measurement of q^* at a lower q-range.

The lamellar periodicity of each diblock sample is plotted as a function of the number-average backbone length L in Figure 4, where L is calculated using a constant contour length of 0.62 nm per poly(norbornene) backbone segment. The relationship $d_0 = 2L$ is also plotted as a blue dotted line, which represents the lamellar period for fully extended bottlebrush molecules packed in an end-to-end bilayer arrangement with negligible end effects. Over the wide range of L shown in Figure 4, it is clear that the average slope between data points on the log−log axes is not constant and continually increases, obviating a fit to the $d_0 \propto L^{\gamma}$ relationship with a constant scaling exponent γ. Instead, the scaling exponent transitions from $\gamma < 0.3$ to a value that approaches unity as L is increased. In particular, a power-law fit to our two largest molecules gives a scaling exponent of $\gamma = 0.88$, which is greater than the scaling of strongly segregated linear diblock polymers ($\gamma = 2/3$).[24] The large scaling exponent is consistent with prior experimental studies that accredited it to highly extended conformations of large, cylindrical bottlebrushes.[8,9,20,22] At small backbone lengths, the scaling exponent decreases considerably. A fit to the smallest two samples yields a scaling exponent of only $\gamma = 0.26$. In this size regime, the molecules no longer resemble cylindrical brushes since the contour lengths of the backbones are shorter than the side chains. In this limit the lamellar period is dominated by the side chain dimensions with only weak dependence on the backbone length, and it actually exceeds the $d_0 = 2L$ line as a consequence. As this line ignores end effects, it loses significance for the more starlike polymers at low L.

Theory Results. Predictions of the lamellar period for each of the diblock bottlebrush polymers were made using the SCFT model described above. The structural input parameters, given in Table 3, were calculated on the basis of the molecular characterizations. The number of branches per block (m_A and m_B) were taken as the number-average degree of polymerization of each block from Table 2, and the number of segments per branch (N_A and N_B) were normalized to a common reference volume of $v_{ref} = 118$ Å^3. Unfortunately, we are not aware of a literature value of χ for PS and aPP, and so we use an estimate based on a literature value for melts of linear PS-*b*-PEP diblock copolymer.[33]

For the segment lengths, we scale the literature values for PS and aPP by a factor of 1.5, on the assumption that the side chains of the bottlebrushes are stretched approximately 50% from their unperturbed length (i.e., from about 4 to 6 nm). This small increase in length has a comparable effect on the lamellar period, which is only significant for our shortest bottlebrushes. It is because of its small effect that we do not have to

TABLE 3. Structural Input Parameters of Diblock Bottlebrush Polymers for SCFT Calculations

sample label	N_A[a]	N_B[a]	m_A[b]	m_B[b]	m[c]	L (nm)[d]	χN[e]	a_A (Å)[f]	a_B (Å)[f]
[P(aPP)-*b*-P(PS)]$_{28.3k}$	34	54	6	4	10	6.3	47	9.2	8.2
[P(aPP)-*b*-P(PS)]$_{41.8k}$	34	51	10	6	16	9.6	70	9.2	8.2
[P(aPP)-*b*-P(PS)]$_{54.2k}$	34	54	12	7	19	12	91	9.2	8.2
[P(aPP)-*b*-P(PS)]$_{95.9k}$	34	51	18	16	34	21	158	9.2	8.2
[P(aPP)-*b*-P(PS)]$_{123k}$	34	51	35	14	49	30	212	9.2	8.2
[P(aPP)-*b*-P(PS)]$_{153k}$	34	54	35	20	55	34	258	9.2	8.2
[P(aPP)-*b*-P(PS)]$_{303k}$	34	51	84	34	118	74	522	9.2	8.2
[P(aPP)-*b*-P(PS)]$_{368k}$	34	54	100	41	141	87	633	9.2	8.2
[P(aPP)-*b*-P(PS)]$_{696k}$	34	54	219	62	281	174	1220	9.2	8.2

[a] Number of segments per aPP branch (N_A) and per PS branch (N_B) based on a 118 Å^3 reference volume. [b] Number of aPP branches per molecule (m_A) and PS branches per molecule (m_B) reported to the nearest integer. [c] Number of total branches per molecule. [d] Backbone contour length calculated by $L = (0.62\ \text{nm} \times m)$, based on a length of 0.62 nm per poly(norbornene) repeat unit. [e] Segregation strength. Initial estimates for these values were based on a PS-*b*-PEP system[33] using $\chi N = X(M_n/\rho RT)$, where $X_{PS-PEP} = 1655/T\ (K) + 0.57$ with $v_{ref} = 118$ Å^3. The values given are 25% greater than the initial estimates and were used for all of the calculations in this report. [f] Statistical segment length used for aPP side chains (a_A) and PS side chains (a_B). These lengths are 50% greater than values reported in the literature[34] in order to account for chain stretching effects.

concern ourselves with a more rigorous treatment for the radial stretching of the side chains.

The backbone persistence length, ξ_b, was the only parameter treated as a fitting parameter. Predictions of d_0 were obtained for eight of the nine samples. (The SCFT calculations were not able to converge on a solution for the largest sample because of numerical difficulties resulting from the extreme level of segregation). The best fit to the data occurred for $\xi_b = 6$ backbone units (3.7 nm). The fit is very good apart from the smallest molecule, for which the SCFT predicts 14.8 nm as compared to the 16.4 nm from the experiment. In the case of small L, the persistence length has a negligible effect on d_0, and so this could be an indication that the scaling factor used for the segment lengths needs to be increased. However, we believe the discrepancy is because our estimation of χ is too small, on account of the fact that it results in a sinusoidal composition profile characteristic of a weakly segregated melt. Therefore, we increased our initial estimate of χ by 25% and repeated the calculations. This time the best fit occurred for $\xi_b = 5$ backbone units (3.1 nm). This set of χ and ξ_b parameters is used for all the remaining calculations in this report, and the resulting predictions for the lamellar periodicity are plotted in Figure 4. A table of SCFT results using four different values of ξ_b and the two values of χ is provided in the Supporting Information.

The agreement of the SCFT predictions with the experimental results is remarkable. Nearly all of the SCFT data points in Figure 4 are within 5% of the experimental values. Consequently, the observed trend of an increasing scaling exponent with increasing L is entirely captured by the theory. It would be preferable if we had a literature value for χ based on PS and aPP, but we are reasonably confident that the correct value lies approximately in the range of the two values we examined. Much smaller and the lamellar phase of our smallest bottlebrush would disorder, while much larger and the level of segregation would not be consistent with the fact that its ODT is experimentally accessible. In any case, the domain size of well-segregated melts of linear diblock is weakly dependent on χ, and the same is true here. In particular, the 25% increase in χ only caused a $\sim$ 3% increase in d_0 for all samples, except for the smallest bottlebrush where d_0 increased by $\sim$6%. This increase in d_0 was then largely compensated for by a slight reduction in ξ_b from 6 to 5 backbone units. Therefore, the agreement with experiment is robust, implying that the model provides an intrinsically good representation of the system. The uncertainty in χ just leads to a modest uncertainty in ξ_b. It is worth noting that recent simulations[35] found that the steric-induced Kuhn length of the backbone, $b_K = 2\xi_b$,[36] is similar to the diameter of the bottlebrush, $2R_g \sim a_A N_A^{1/2} \sim a_B N_B^{1/2}$. As it turns out, these two quantities are also comparable in our system (both $\sim$6 nm) for either of our estimates of ξ_b.

The success of the SCFT in predicting the experimental domain spacing is encouraging and allows us to confidently use the theory to study the details of the molecular self-assembly. We first calculated composition profiles to examine the degree of segregation in the melt. Figure 5 compares the relative A-segment concentration, $\phi_A(z)$, over one lamellar period for four of the diblock samples. The domains of our shortest bottlebrush, [P(aPP)-*b*-P(PS)]$_{28.3k}$, contain a small but noticeable amount of the other component at their centers (i.e., 1%), and therefore, we regard this sample as intermediately segregated. This is consistent with our ability to access the T_{ODT} of this polymer. The domains of the larger molecules become essentially pure, resulting in profiles that are more square-wave in nature. Therefore, these can be unambiguously classified as strongly segregated. However, the increased segregation does not imply that A/B interfaces are narrower. Figure 5b shows that the interfacial profiles in absolute units are virtually identical, with a common interfacial width of $w_{int} = 2.1$ nm, as determined by the dashed tangent line. Just as for conventional linear diblock copolymers, the interface is well approximated by that of a strongly segregated binary homopolymer blend. Indeed, our interfacial width is indistinguishable from the theoretical prediction $w_{int} = [(a_A^2 + a_B^2)/3\chi]^{1/2}$ for the homopolymer blend.[37]

To help understand how the bottlebrush molecules pack within the lamellar phase, we calculated the joint-distribution function, $p_{A,i}(z,u)$, for the position, z, and orientation, u, of the ith backbone unit along the A-block. The units are numbered sequentially from $i = 1$ at the A-B block junction to $i = m_A$ at the A-end

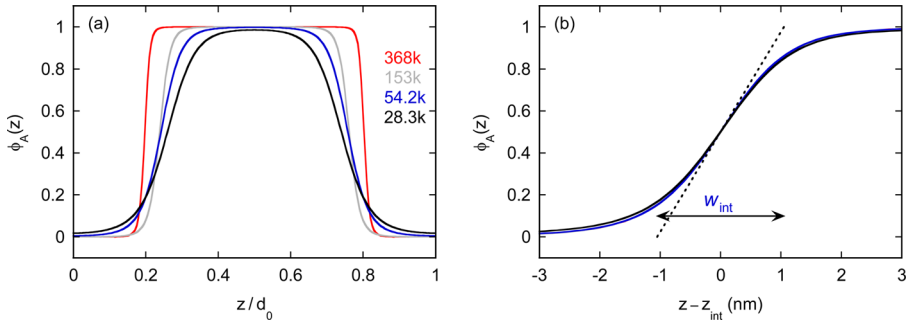

Figure 5. Composition profiles of four diblock samples plotted (a) in relative units over one complete lamellar period and (b) in absolute units centered about an A/B interface, z_{int}. The dashed line coincides with the predicted[37] interfacial width, $w_{int} = [(a_A^2 + a_B^2)/3\chi]^{1/2}$.

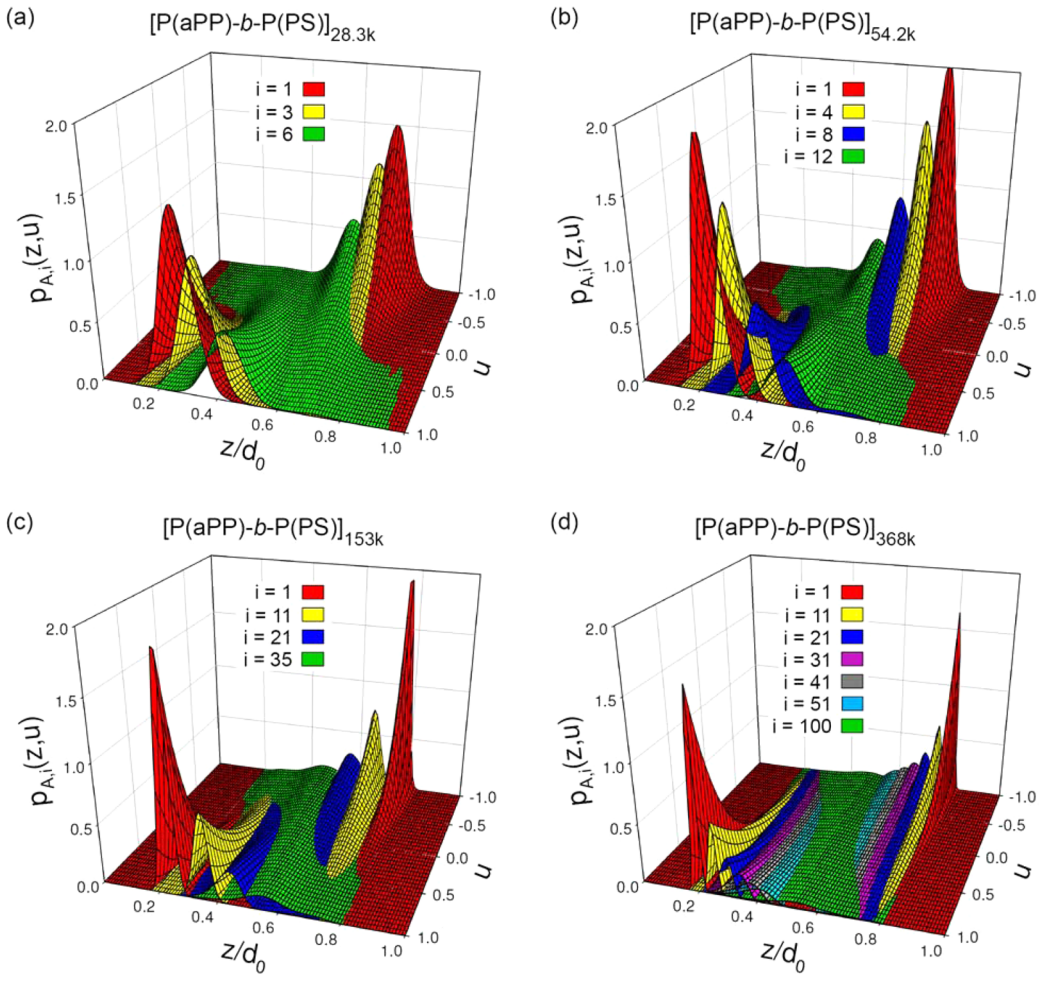

Figure 6. SCFT results for the four bottlebrushes considered in Figure 5 showing the joint-distribution function, $p_{A,i}(z,u)$, for the position, z, and orientation, $u = \cos(\theta)$, of various individual backbone segments, i, along the A-block. The distributions are normalized such that $\int p_{A,i}(z, u)\, dz\, du = 1$. Note that the final distribution in each plot (shown in green) corresponds to the terminal backbone units since $m_A = 6$, 12, 35, and 100 for the bottlebrushes in plots (a), (b), (c), and (d), respectively.

of the backbone. Here we follow the standard convention of specifying the orientation of the backbone by $u = \cos(\theta)$, where θ is the angle of the backbone relative to the lamellar normal. Figure 6 shows $p_{A,i}(z,u)$ at various points along the A-block for the same four molecules considered in Figure 5. The dominant features are the two strong peaks for the $i = 1$ units. The peaks at $z/d_0 \approx 1/4$ and $u = \cos(0°) = 1$ indicate that the backbone junctions are highly localized at the interface and strongly oriented normal to the lamellae. Similarly, the peaks at $z/d_0 \approx 3/4$ and $u = \cos(180°) = -1$ indicate an equivalent localization at the neighboring interface but with the opposite orientation. As i increases, the distributions shift toward the center of the A-domains

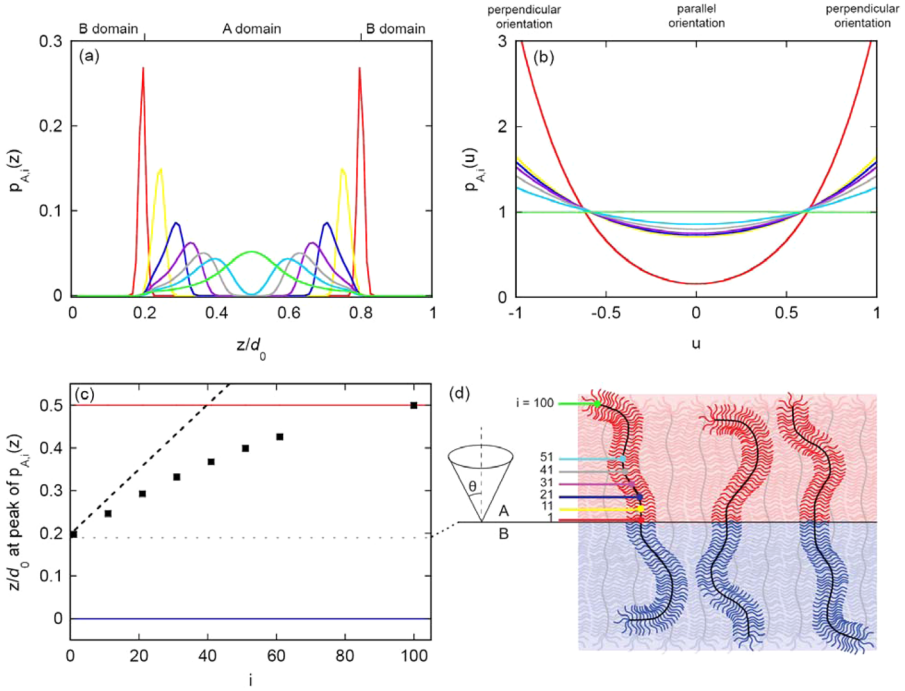

Figure 7. Probability distributions for A-block backbone segments, *i*, of [P(aPP)-*b*-P(PS)]$_{368k}$ calculated by SCFT. Backbone segments range from *i* = 1 to *i* = 100, indicating their distance from the A−B block junction. Different colored traces in plots (a) and (b) represent different backbone segments as defined in plot (d). (a) Positional probability distribution, $p_{A,i}(z)$, of backbone segments within the A-domain. (b) Orientational probability distribution, $p_{A,i}(u)$, of backbone segments relative to the A/B interface. (c) Most probable positions of backbone segments (black squares). The dashed black line indicates the maximum progression of backbone locations for a fully extended chain. The red and blue solid lines denote the center of the A-domain and B-domain, respectively, while the dotted line designates the A/B interface. (d) Graphic defining A-block backbone segments and the backbone orientation angle, θ.

(i.e., $z/d_0 = 1/2$) and broaden in both the z and u directions, indicating a reduction in localization and orientation, respectively.

The 3D plots in Figure 6 provide a detailed picture of the molecular packing for bottlebrush block polymers of increasing backbone lengths. To highlight the assembly behavior of our most brushlike molecules, individual distributions of z and u for various values of i (see color legend) are plotted in Figure 7 for [P(aPP)-*b*-P(PS)]$_{368k}$, which is the largest bottlebrush that was modeled. Figure 7a shows the positional probability, $p_{A,i}(z)$, obtained by integrating $p_{A,i}(z,u)$ over all orientations, $u = -1$ to 1. This plot clearly shows the strong localization of the junctions ($i = 1$) at the two interfaces and the subsequent delocalization and progression toward the center of the A-domain with successive steps along the A-block in units of the Kuhn length (i.e., $\Delta i = 10$, since $b_K = 2\xi_b$ and $\xi_b = 5i$). By five Kuhn lengths ($i = 51$), or halfway along the A-block, the distributions originating from the two neighboring interfaces are beginning to overlap in the middle of the A-domain. Figure 7b shows the orientation probability, $p_{A,i}(u)$, obtained by integrating $p_{A,i}(z,u)$ over one lamellar period, $z = 0$ to d_0. The junction point ($i = 1$) is highly oriented due to the strong gradient in the composition profile, but this orientational order quickly fades within a few units along the backbone as it exits the interfacial region. (Recall that the length of a backbone unit is 0.62 nm, which is comparable to the interfacial width in Figure 5b). The rapid decrease in orientational order is followed by a more gradual decrease to the point where the end of the A-block ($i = 100$) shows a relatively flat distribution, implying that all orientations are equally probable. Figure 7c displays the most probable location (i.e., the peak in $p_{A,i}(z)$) of several backbone units along the A-block. The dashed line denotes the maximum possible progression of the backbone position corresponding to a fully extended chain. The data initially progress closely with this theoretical maximum, consistent with the high degree of orientation near $i = 1$. However, the progression slows as the backbone becomes less oriented. Ultimately, the end of the backbone ($i = 100$) gives a symmetric positional distribution centered in the middle of the A-domain.

We now examine how the length of the backbone affects the arrangement of the bottlebrushes within the lamellar phase by inspecting the other 3D plots in Figure 6, along with the corresponding plots of $p_{A,i}(z)$ and $p_{A,i}(u)$ provided in the Supporting Information. It is clear from these plots that the backbone orientation of the [P(aPP)-*b*-P(PS)]$_{153k}$ bottlebrushes vanishes toward their ends, much like that of [P(aPP)-*b*-P(PS)]$_{368k}$. However, the shorter [P(aPP)-*b*-P(PS)]$_{54.2k}$ molecules maintain a significant degree of orientation along their

entire A-block. This is not too surprising since the A-block is only a single Kuhn length. Consequently, the ends of the A-blocks are much more localized at the center of the A-domain and have a reasonable preference for the $u = \pm 1$ orientations (see Figure 6b). Due to their more extended conformations, the lamellar period of $[P(aPP)\text{-}b\text{-}P(PS)]_{54.2k}$ approaches the blue dashed line ($d_0 = 2L$) in Figure 4. Furthermore, for our shortest $[P(aPP)\text{-}b\text{-}P(PS)]_{28.3k}$ molecules where the A-block is only half a Kuhn length, the lamellar period actually exceeds $d_0 = 2L$. This implies that the backbones are too short to reach the middle of the A-domain. Indeed, the separate peaks in $p_{A,i}(z)$ from molecules at the adjacent interfaces do not converge at the center of the A-domain even for $i = m_A = 6$ (see Figure 6a). Instead, the side chains have to extend beyond the ends of the backbone to fill the middle of the domains. This is consistent with our characterization of molecules with short backbones as conformationally starlike.

Discussion. The quantitative agreement between our experiment and SCFT allows us to challenge the prevailing belief that bottlebrush block polymers in an ordered lamellar state are highly extended in an orientation perpendicular to the lamellar plane. The only experimental evidence for this is the near-linear dependence of the domain spacing, d_0, with the molar mass (or DP) of the molecule. There are two space-filling ways for this to occur: either a bilayer arrangement with each block extending halfway across its respective domain or an interdigitated arrangement where each block extends completely across the domain. Apart from small deviations due to bending of the molecules and end effects, the domain spacing of these two possibilities would obey $d_0 = 2L$ and $d_0 = L$, respectively. In either case, d_0 scales linearly with L, which is proportional to DP. Surprisingly, the only previous study to report how the lamellar period compared with the length of a bottlebrush molecule was that of Xia et al.[9] The authors found that $d_0 \approx L$ and concluded that the molecular packing was interdigitated. However, no explanation was given as to why the molecules would pack this way. We posit that this type of packing is unlikely because interdigitation doubles the number of interfaces while offering no obvious free energy gain to compensate for the increase in interfacial energy. Gu et al. have suggested the bilayer arrangement, but without confirming that their experimental data satisfied $d_0 \approx 2L$.[22] This conclusion was instead based on simulations, which predicted the ends of the backbone to be concentrated in the middle of the domains, consistent with our SCFT results.

Our study is the first to pay particular attention to how the lamellar period compares to the extended length of the backbone. Apart from our smallest molecules, d_0 is significantly less than $2L$ implying that the bottlebrushes are not highly extended. Of course, very short molecules will have extended backbones when the persistence length of the backbone is comparable to its length, which explains why d_0 is closer to $2L$ for short molecules. The fact that d_0 actually exceeds $2L$ for our smallest molecule is also easily explained. When the backbone becomes short relative to the side chains, the molecules start to resemble heteroarm star-block copolymers. Consequently, d_0 is then dictated by the length of the side chains rather than the backbone, which in turn implies that the exponent γ must approach zero in the limit of small L. This is consistent with our results in Figure 4. The reduction in γ may also provide an explanation for previous experimental results by Gu et al. in which two distinct series of symmetric diblock bottlebrush polymers were synthesized with PS and polylactide (PLA) side chains.[22] The first series involved 2.4 kg/mol side chains on both blocks while the second series had blocks with ~4.5 kg/mol side chains. Both series where fit to a power law $d_0 \sim DP^{\gamma}$ assuming a constant exponent, γ, and the first series was found to exhibit a greater scaling exponent than the second series. The range of backbone DP in that study did not extend as low as our samples, but it may have been low enough to be effected by the finite length of the side chains relative to L. Naturally, the bottlebrushes with the longer side chains would have been affected by a greater degree, which could explain the slightly smaller exponent obtained for the second series of bottlebrushes.

For our larger molecules, where the length of the side chains is small relative to the backbone, we obtained results that are consistent with previous experimental studies. As was the case in the study by Xia et al.,[9] our lamellar periods are similar to the length of the backbone, $d_0 \approx L$. However, as clearly illustrated by our SCFT calculations, the reason is not the interdigitation of highly extended chains. Rather, it is because of the significant bending of the molecules. Furthermore, our exponent $\gamma = 0.88$ at large L is similar to the exponents $\gamma = 0.91$ and 0.84 reported by Gu et al. for their two different bottlebrush series.[22] Although these exponents are larger than those of linear diblocks, presumably because of the effective stiffness of the backbone due to crowding of the side chains, they are still less than unity, which is expected for highly extended conformations. Of course, the exponent is not universal and would likely adopt values closer to 1 for bottlebrushes with more crowded side chains. Note that Hong et al.[38] have reported exponents very close to 1, but this was for thin films where the bottlebrush assembly was constrained by a substrate that may have restricted their bending, thus resulting in more extended conformations and larger exponents.

Although the bottlebrushes produce significantly larger exponents than their linear counterparts, they should eventually behave the same in the limit of

large L. Ultimately, the persistence length and diameter of the bottlebrush will become negligible relative to L, and the bottlebrush will begin to resemble a very large linear diblock with Gaussian statistics. Thus, the exponent should eventually decrease toward $\gamma = 2/3$, and the lamellar period should become small relative to L. It is unlikely that experiments would be able to access the equilibrium behavior in this extreme limit, but it may be possible to reach molar masses where the exponent starts to decrease.

CONCLUSIONS

We have developed the first quantitative theory for the melt state of bottlebrush block polymers and have validated its predictions with experimental results. Specifically, we synthesized nine lamellar-forming bottlebrush diblock polymers of different lengths, L, and determined their lamellar periods, d_0, using SAXS measurements. The scaling $d_0 \propto L^{\gamma}$ exhibited a variable exponent ranging from $\gamma < 0.3$ at small L and approaching $\gamma = 1$ at high L. We attribute this behavior to the transition from starlike to brushlike molecules as the backbone becomes long relative to the length of the side chains. The actual molecular parameters associated with the block polymer samples were then used to define the input parameters for the theoretical calculations, resulting in remarkable quantitative agreement between the theoretical predictions of the lamellar domain spacing and the experimental data. These theoretical results conclusively establish the molecular origins of the domain scaling behavior of lamellar forming diblock bottlebrush polymers.

Our SCFT approach is based on a realistic microscopic model capable of explicitly incorporating the large number of branches (or side chains) characteristic of bottlebrush molecules. However, the crowding of the densely packed branches results in strong steric interactions, which would normally be overlooked by a SCFT calculation. The stretching of the side chains radially outward from the backbone is a minor effect for large bottlebrushes, and so we account for it by simply scaling their segment lengths by a physically reasonable factor of 1.5. The strong correlations between a backbone and its grafted branches imply that a mean-field treatment of its interactions would be inappropriate. However, the interaction energy should be relatively constant, and thus this issue is resolved by simply omitting all interactions involving the backbone. Lastly, the lateral pressure that tends to extend the backbone and restrict its flexibility is accounted for by modeling the backbone as a semiflexible wormlike chain with an adjustable persistence length, ξ_b, which we treat as a fitting parameter. Apart from ξ_b and the scaling factor for the segment lengths, all the model parameter can in principle be determined from experiment. In our case, we did not have an accurate estimate of the interaction χ parameter for PS and aPP, but fortunately d_0 is relatively insensitive to χ and adjusting ξ_b readily compensates for small inaccuracies in χ.

The close agreement between theory and experiment was achieved using a persistence length of $\xi_b = 5$ backbone units (i.e., 3.1 nm). This result implies that bottlebrushes are more flexible in the melt state than generally assumed, consistent with recent simulations by Cao et al.[35] who find that the effective Kuhn length of the backbone ($b_K = 2\xi_b$) in the melt is comparable to the diameter of the bottlebrush. Such macromolecular flexibility directly influences packing of the bottlebrushes within the lamellar morphology. Contrary to the generally accepted hypothesis that the chains are highly extended in either an interdigitated (i.e., $d_0 \approx L$) or end-to-end bilayer (i.e., $d_0 \approx 2L$) arrangement, our calculations predict considerable bending of the backbones. Although the backbones are highly oriented at the A−B block junction, the orientational order drops off precipitously as the molecules emerge from the interfacial region. A more gradual decline in orientation follows within the essentially pure A and B domains of the high molar mass diblocks, and the ends of the backbones show broad positional distributions with no orientational preference. This behavior is indicative of a random walk, albeit with a sizable step size (or Kuhn length).

This investigation highlights the importance of combining the development of state-of-the-art theory with advances in experimental polymer science. The iterative interplay between the theoretical model presented here, and the synthesis and characterization of a judiciously chosen set of model materials, has produced definitive explanations for the self-assembly behavior of bottlebrush block polymers.

MATERIALS AND METHODS

Materials. All chemical reagents were purchased from Sigma-Aldrich and used as received unless otherwise specified. Styrene and ethylene oxide for anionic polymerization were purified using previously reported techniques.[39] Styrene monomer for RAFT polymerization was purified by passing through a plug of basic alumina to remove inhibitor. The aPP-NB macromonomer was prepared by chemical modification of a vinyl-terminated aPP starting material (provided by ExxonMobil Chemical Company) according to procedures detailed elsewhere.[40]

Molecular Characterization. Nuclear magnetic resonance (^{1}H NMR) measurements were taken on a Bruker Avance III 500 MHz spectrometer. Molecular characterization of bottlebrush polymers was primarily conducted using size exclusion chromatography with multiangle laser light scattering detection (SEC-MALLS). Samples were analyzed at 25 °C in a tetrahydrofuran mobile phase at 1.0 mL/min using an Agilent 1260 Infinity LC system equipped with three Waters Styragel columns in series,

a Wyatt OPTILAB T-rEX refractive index (RI) detector, and a Wyatt DAWN Heleos II 18-angle laser light scattering detector. The aPP-block of each diblock was characterized by SEC-MALLS analysis of an aliquot removed from the polymerization and terminated immediately before adding the PS-NB macromonomer to the reaction flask. The absolute molar mass and volume fraction of the final diblock polymers were then determined using dn/dc values measured with the SEC instrument assuming 100% mass elution. This value was usually very close to the estimate calculated with a mass average of the pure component values (dn/dc_{aPP} = 0.079 mL/g and dn/dc_{PS} = 0.185) using dn/dc = [w_{aPP}(dn/dc_{aPP})] + [w_{PS}(dn/dc_{PS})], where w_{aPP} and w_{aPP} are the feed weight fractions of each component.

SAXS Analysis and Sample Preparation. SAXS experiments were conducted at the Advanced Photon Source at Argonne National Laboratory on the DND-CAT beamline (Sector 5-ID-D). Two-dimensional SAXS patterns were acquired with a Rayonix area CCD detector using a sample-to-detector distance of 8.5 m. Patterns were azimuthally integrated to give one-dimensional plots of intensity versus q. X-rays of wavelength λ = 0.729 Å were used for all samples except for [P(aPP)-*b*-P(PS)]$_{696k}$, which used X-rays of λ = 1.24 Å to measure a lower q-range. Exposure times of either 1 or 2 s were used for all measurements. Samples were initially prepared by solvent casting. About 75 mg of each sample was dissolved in tetrahydrofuran in 5 mL PTFE beakers, and the solvent was allowed to slowly evaporate over several days. To maintain a slow evaporation rate, the beakers were kept in a loosely covered Pyrex dish with ~1 cm of tetrahydrofuran coating the bottom. The films were then dried under vacuum, loaded into aluminum DSC pans, hermetically sealed in a glovebox under a nitrogen atmosphere, and thermally annealed at 150 °C for 4 h. The samples were heated back to 150 °C on the beamline using a Linkam hot stage equipped with liquid nitrogen cooling and equilibrated for 3−5 min before taking measurements. Variable temperature SAXS measurements were carried out for two of the samples to determine T_{ODT} values (see Figure 2). Fast heating rates were used between temperatures (>100 °C/min), and the samples were held at each temperature for 2−5 min to equilibrate before taking measurements.

Synthesis. Diblock bottlebrush polymers were synthesized by sequential addition of aPP-NB and PS-NB macromonomers to a living ROMP initiated with Grubbs third generation catalyst (Figure 1). The same aPP-NB macromonomer batch was used for all nine diblock polymers in this report, and details for aPP-NB synthesis are outlined in ref 40. Alternatively, two different PS-NB macromonomer batches with molar masses of 4.0 kg/mol and 3.8 kg/mol were prepared via anionic polymerization and reversible addition−fragmentation chain transfer (RAFT) polymerization, respectively. Synthetic procedures for both PS-NB batches are detailed below. Additional schemes and characterization of these reactions are provided in the Supporting Information.

Synthesis of PS-NB(4.0k). ω-Hydroxyl polystyrene (PS−OH; M_n = 3.8 kg/mol by ^{1}H NMR) was initially synthesized by anionic polymerization of styrene following well-known procedures and purified by freeze-drying from a benzene solution. The PS−OH was then functionalized using the following process. A flame-dried round-bottom flask was charged with *exo*-5-norbornenecarboxylic acid (460 mg, 3.3 mmol) and consecutive vacuum/argon cycles were carried out to remove air from the headspace. The solid *exo*-5-norbornenecarboxylic acid was dissolved with degassed toluene (5 mL), and oxalyl chloride was slowly injected with constant stirring. A bubbler attached to the argon line in the back of the hood was used to relieve excess pressure in the system. The reaction was stirred at room temperature for 30 min and then at 70 °C for 2 h. The mixture was then cooled to 0 °C using an ice bath. In a separate flask, a solution of PS−OH (2.46 g, 0.65 mmol), triethylamine (0.5 mL, 3.6 mmol), and toluene (20 mL) were degassed via freeze−pump−thaw cycles. This solution was cannulated into the reaction flask at 0 °C. After about 5 min, the reaction flask was heated slowly to 100 °C and stirred for 18 h. Finally, the solution was cooled to room temperature, filtered twice to remove salts, and precipitated into methanol (400 mL).

Synthesis of Norbornene-Functionalized RAFT Agent. S-Dodecyl-*S*′-(α,α′-dimethyl-α″-acetic acid)trithiocarbonate (TTC-acid; 1.30 g, 3.57 mmol) was loaded into a flame-dried 25 mL Schlenk flask and sealed with a rubber septum. Air was removed from the flask using consecutive vacuum-argon cycles and left under positive argon pressure. Oxalyl chloride (3.25 mL, 37.9 mmol) was injected with rapid stirring. The flask was connected to a bubbler and argon was allowed to flow through the flask headspace. After a few minutes, the TTC-acid became completely dissolved and the argon flow was ceased. Reaction progress was then monitored by evolution of gaseous byproducts (CO_2, CO, and HCl) from the bubbler. After stirring for 3 h, excess oxalyl choride was removed in vacuo. Once the resulting acyl chloride product was dried, the flask was recharged with positive argon pressure and *exo*-5-norbornene-2-methanol (0.43 mL, 3.57 mmol) was added via syringe while stirring. The solution quickly began bubbling with HCl (g) generation. After 1 h the bubbler was removed and the solution was allowed to stir under an argon atmosphere overnight. After 14 h, the flask was opened to air. Isopropanol (2 mL) was added and stirred for 2.5 h before removing under reduced pressure, yielding a dark yellow oil as the crude product. This product was purified by elution through a silica column (30 mm diameter column loaded with ~30 g silica gel) using a 50/50 hexanes/dichloromethane (v/v) mixture and collecting 5 mL fractions. The pure TTC-NB product was eluted in fractions 8−20 as confirmed by ^{1}H NMR and collected by rotary evaporation. Yield: 1.23 g.

Synthesis of PS-NB(3.8k). TTC-NB (0.8 g, 1.7 mmol), azobis(isobutyronitrile) (AIBN; 27.8 mg, 0.17 mmol), and purified styrene (9.4 mL, 82.1 mmol) were mixed into a flame-dried 50 mL Schlenk flask and the solution was degassed by three consecutive freeze−pump−thaw cycles. Following the final cycle, the reaction flask was backfilled with positive argon pressure. The solution was then heated to 70 °C and stirred under an argon atmosphere for several hours. Reaction progress was monitored by ^{1}H NMR analysis of removed aliquots. The polymerization was terminated at ~75% conversion by quenching in liquid N_2, opening the solution to air, and precipitating in methanol. Yield: 4.92 g.

Synthesis of Diblock Bottlebrush Polymers via Sequential ROMP of Macromonomers. In a typical reaction, aPP-NB and PS-NB (~200 mg each depending on the target volume fraction) were loaded into separate oven-dried scintillation vials and brought into a glovebox. Under a nitrogen atmosphere, both macromonomers were dissolved in degassed tetrahydrofuran (50 mg/mL). In a separate scintillation vial, a desired amount of Grubbs third generation catalyst (G3) was dissolved in ~1 mL of tetrahydrofuran, and the aPP-NB solution was quickly added to the catalyst solution while stirring to initiate polymerization of block A. After 3−5 min (depending on target molecular weight) an aliquot was taken to characterize the first block, the PS-NB solution was added, and the reaction mixture was stirred for ~1 h. The reaction was terminated with excess ethyl vinyl ether, stirred for >30 min, and precipitated into methanol. After drying under high vacuum, some of the samples revealed unreacted PS-NB macromonomers in the SEC traces. This may indicate the presence of unfunctionalized macromonomer chains. To remove unreacted PS macromonomers, the diblock products were stirred in ~10 mL of acetone for several hours. The acetone was then decanted away from the nondissolved polymer. The remaining product was again dried, and SEC analysis revealed that the fraction of low molar mass chains had either been reduced or completely removed.

Theoretical Calculations. Our model, which is fully defined by the description in the Theory Model section, is solved using the well-established procedures of self-consistent field theory (SCFT).[28,29] Since interactions involving the backbone are ignored, there are only fields acting on the A and B segments, $w_A(\mathbf{r})$ and $w_B(\mathbf{r})$, respectively. The first step in the calculation is to calculate a pair of partial partition functions (or propagators) for each block of the molecule, one for each direction along the chain. The fields enter the simpler diffusion equation for the Gaussian side chains, whereas the more complicated diffusion equation for the wormlike backbone is solved without a field. The connectivity of the molecule is incorporated through the initial conditions of the propagators. The concentration of each

block is then obtained by integrating the product of its propagators along its contour. Because we are ignoring the volume of the backbone, we only need the total concentrations of the A and B side chains, $\phi_A(\mathbf{r})$ and $\phi_B(\mathbf{r})$, respectively. The next step in the calculation is to adjust $w_A(\mathbf{r})$ and $w_B(\mathbf{r})$ so as to satisfy the self-consistent field conditions, $w_A(\mathbf{r}) - w_B(\mathbf{r}) = \chi N[\phi_B(\mathbf{r}) - \phi_A(\mathbf{r})]$ and $\phi_A(\mathbf{r}) + \phi_B(\mathbf{r}) = 1$, where $N = m_A N_A + m_B N_B$ is the total polymerization of the bottlebrush. Lastly, we minimize the free energy to obtain the equilibrium lamellar period, d_0.

There are numerous numerical methods for solving the diffusion equations. We use the spectral method as described in ref 41 for Gaussian chains and in ref 42 for wormlike chains. Likewise, there are different methods for satisfying the self-consistent field conditions. Here, this is done with the Anderson-mixing scheme as specified in ref 43. The minimization of the free energy is performed by a simple Newton–Raphson iteration.

Conflict of Interest: The authors declare no competing financial interest.

Acknowledgment. We acknowledge ExxonMobil Chemical Company for providing vinyl-terminated aPP starting material and financial support for this work. Support from the Center for Sustainable Polymers at the University of Minnesota, a National Science Foundation (NSF)-supported Center for Chemical Innovation (CHE-1413862) is also acknowledged. Portions of the work were performed at the DuPont–Northwestern–Dow Collaborative Access Team (DND-CAT) located at Sector 5 of the Advanced Photon Source (APS). DND-CAT is supported by The Dow Chemical Company, E.I. DuPont de Nemours & Co., and Northwestern University. Use of the APS, an Office of Science User Facility operated for the U.S. Department of Energy (DOE) Office of Science by Argonne National Laboratory, was supported by the U.S. DOE under Contract DE-AC02-06CH11357. We also thank Morgan Schulze for her assistance in macromonomer synthesis, and Justin Bolton for helpful discussions regarding bottlebrush polymer synthesis techniques.

Supporting Information Available: The Supporting Information is available free of charge on the ACS Publications website at DOI: 10.1021/acsnano.5b05473.

Additional SCFT results and SAXS data, ^{1}H NMR spectra of macromonomers, SEC traces of bottlebrush polymers, and detailed comparison of ROMP catalysts (PDF)

REFERENCES AND NOTES

1. Verduzco, R.; Li, X.; Pesek, S. L.; Stein, G. E. Structure, Function, Self-Assembly, and Applications of Bottlebrush Copolymers. *Chem. Soc. Rev.* **2015**, *44*, 2405–2420.
2. Rzayev, J. Molecular Bottlebrushes: New Opportunities in Nanomaterials Fabrication. *ACS Macro Lett.* **2012**, *1*, 1146–1149.
3. Sheiko, S. S.; Sumerlin, B. S.; Matyjaszewski, K. Cylindrical Molecular Brushes: Synthesis, Characterization, and Properties. *Prog. Polym. Sci.* **2008**, *33*, 759–785.
4. Gerle, M.; Fischer, K.; Roos, S.; Müller, A. H. E.; Schmidt, M.; Sheiko, S. S.; Prokhorova, S.; Möller, M. Main Chain Conformation and Anomalous Elution Behavior of Cylindrical Brushes as Revealed by GPC/MALLS, Light Scattering, and SFM. *Macromolecules* **1999**, *32*, 2629–2637.
5. Lecommandoux, S.; Chécot, F.; Borsali, R.; Schappacher, M.; Deffieux, A.; Brûlet, A.; Cotton, J. P. Effect of Dense Grafting on the Backbone Conformation of Bottlebrush Polymers: Determination of the Persistence Length in Solution. *Macromolecules* **2002**, *35*, 8878–8881.
6. Sun, G.; Cho, S.; Clark, C.; Verkhoturov, S. V.; Eller, M. J.; Li, A.; Pavía-Jiménez, A.; Schweikert, E. A.; Thackeray, J. W.; Trefonas, P.; et al. Nanoscopic Cylindrical Dual Concentric and Lengthwise Block Brush Terpolymers as Covalent Preassembled High-Resolution and High-Sensitivity Negative-Tone Photoresist Materials. *J. Am. Chem. Soc.* **2013**, *135*, 4203–4206.
7. Macfarlane, R. J.; Kim, B.; Lee, B.; Weitekamp, R. A.; Bates, C. M.; Lee, S. F.; Chang, A. B.; Delaney, K. T.; Fredrickson, G. H.; Atwater, H. A.; et al. Improving Brush Polymer Infrared One-Dimensional Photonic Crystals via Linear Polymer Additives. *J. Am. Chem. Soc.* **2014**, *136*, 17374–17377.
8. Sveinbjörnsson, B. R.; Weitekamp, R. A.; Miyake, G. M.; Xia, Y.; Atwater, H. A.; Grubbs, R. H. Rapid Self-Assembly of Brush Block Copolymers to Photonic Crystals. *Proc. Natl. Acad. Sci. U. S. A.* **2012**, *109*, 14332–14336.
9. Xia, Y.; Olsen, B. D.; Kornfield, J. A.; Grubbs, R. H. Efficient Synthesis of Narrowly Dispersed Brush Copolymers and Study of Their Assemblies: The Importance of Side Chain Arrangement. *J. Am. Chem. Soc.* **2009**, *131*, 18525–18532.
10. Miyake, G. M.; Weitekamp, R. A.; Piunova, V. A.; Grubbs, R. H. Synthesis of Isocyanate-Based Brush Block Copolymers and Their Rapid Self-Assembly to Infrared-Reflecting Photonic Crystals. *J. Am. Chem. Soc.* **2012**, *134*, 14249–14254.
11. Li, X.; Prukop, S. L.; Biswal, S. L.; Verduzco, R. Surface Properties of Bottlebrush Polymer Thin Films. *Macromolecules* **2012**, *45*, 7118–7127.
12. Zhang, H.; Zhang, Z.; Gnanou, Y.; Hadjichristidis, N. Well-Defined Polyethylene-Based Random, Block, and Bilayered Molecular Cobrushes. *Macromolecules* **2015**, *48*, 3556–3562.
13. Onbulak, S.; Rzayev, J. Cylindrical Nanocapsules From Photo-Cross-Linkable Core–Shell Bottlebrush Copolymers. *Polym. Chem.* **2015**, *6*, 764–771.
14. Kim, J. G.; Coates, G. W. Synthesis and Polymerization of Norbornenyl-Terminated Multiblock Poly(cyclohexene carbonate)s: A Consecutive Ring-Opening Polymerization Route to Multisegmented Graft Polycarbonates. *Macromolecules* **2012**, *45*, 7878–7883.
15. Tang, H.; Li, Y.; Lahasky, S. H.; Sheiko, S. S.; Zhang, D. Core–Shell Molecular Bottlebrushes with Helical Polypeptide Backbone: Synthesis, Characterization, and Solution Conformations. *Macromolecules* **2011**, *44*, 1491–1499.
16. Huang, K.; Rzayev, J. Well-Defined Organic Nanotubes From Multicomponent Bottlebrush Copolymers. *J. Am. Chem. Soc.* **2009**, *131*, 6880–6885.
17. Cheng, C.; Qi, K.; Khoshdel, E.; Wooley, K. L. Tandem Synthesis of Core–Shell Brush Copolymers and Their Transformation to Peripherally Cross-Linked and Hollowed Nanostructures. *J. Am. Chem. Soc.* **2006**, *128*, 6808–6809.
18. Runge, M. B.; Lipscomb, C. E.; Ditzler, L. R.; Mahanthappa, M. K.; Tivanski, A. V.; Bowden, N. B. Investigation of the Assembly of Comb Block Copolymers in the Solid State. *Macromolecules* **2008**, *41*, 7687–7694.
19. Runge, M. B.; Bowden, N. B. Synthesis of High Molecular Weight Comb Block Copolymers and Their Assembly Into Ordered Morphologies in the Solid State. *J. Am. Chem. Soc.* **2007**, *129*, 10551–10560.
20. Rzayev, J. Synthesis of Polystyrene–Polylactide Bottlebrush Block Copolymers and Their Melt Self-Assembly Into Large Domain Nanostructures. *Macromolecules* **2009**, *42*, 2135–2141.
21. Bolton, J.; Bailey, T. S.; Rzayev, J. Large Pore Size Nanoporous Materials From the Self-Assembly of Asymmetric Bottlebrush Block Copolymers. *Nano Lett.* **2011**, *11*, 998–1001.
22. Gu, W.; Huh, J.; Hong, S. W.; Sveinbjornsson, B. R.; Park, C.; Grubbs, R. H.; Russell, T. P. Self-Assembly of Symmetric Brush Diblock Copolymers. *ACS Nano* **2013**, *7*, 2551–2558; *ACS Nano* **2015**, *9*, 7729.
23. Chremos, A.; Theodorakis, P. E. Morphologies of Bottle-Brush Block Copolymers. *ACS Macro Lett.* **2014**, *3*, 1096–1100.
24. Semenov, A. N. Contribution to the Theory of Microphase Layering in Block-Copolymer Melts. *Sov. Phys. JETP* **1985**, *61*, 733–742.
25. Fredrickson, G. H. Surfactant-Induced Lyotropic Behavior of Flexible Polymer Solutions. *Macromolecules* **1993**, *26*, 2825–2832.
26. Mikhaylov, I. V.; Darinskii, A. A. Effect of the Side-Arm Architecture on the Conformational Properties of Bottle Brushes. *Polym. Sci., Ser. A* **2015**, *57*, 239–250.
27. Saitô, N.; Takahashi, K.; Yunoki, Y. The Statistical Mechanical Theory of Stiff Chains. *J. Phys. Soc. Jpn.* **1967**, *22*, 219–226.

28. Matsen, M. W. The Standard Gaussian Model for Block Copolymer Melts. *J. Phys.: Condens. Matter* **2002**, *14*, R21–R47.
29. Fredrickson, G. *The Equilibrium Theory of Inhomogeneous Polymers*; Oxford University Press: New York. 2006.
30. Xia, Y.; Kornfield, J. A.; Grubbs, R. H. Efficient Synthesis of Narrowly Dispersed Brush Polymers via Living Ring-Opening Metathesis Polymerization of Macromonomers. *Macromolecules* **2009**, *42*, 3761–3766.
31. Li, Z.; Zhang, K.; Ma, J.; Cheng, C.; Wooley, K. L. Facile Syntheses of Cylindrical Molecular Brushes by a Sequential RAFT and ROMP "Grafting-Through" Methodology. *J. Polym. Sci., Part A: Polym. Chem.* **2009**, *47*, 5557–5563.
32. Love, J. A.; Morgan, J. P.; Trnka, T. M.; Grubbs, R. H. A Practical and Highly Active Ruthenium-Based Catalyst That Effects the Cross Metathesis of Acrylonitrile. *Angew. Chem., Int. Ed.* **2002**, *41*, 4035–4037.
33. Lai, C.; Russel, W. B.; Register, R. A.; Marchand, G. R.; Adamson, D. H. Phase Behavior of Styrene−Isoprene Diblock Derivatives with Varying Conformational Asymmetry. *Macromolecules* **2000**, *33*, 3461–3466.
34. Fetters, L. J.; Lohse, D. J.; Richter, D.; Witten, T. A.; Zirkel, A. Connection Between Polymer Molecular Weight, Density, Chain Dimensions, and Melt Viscoelastic Properties. *Macromolecules* **1994**, *27*, 4639–4647.
35. Cao, Z.; Carrillo, J.-M. Y.; Sheiko, S. S.; Dobrynin, A. V. Computer Simulations of Bottle Brushes: From Melts to Soft Networks. *Macromolecules* **2015**, *48*, 5006–5015.
36. Hiemenz, P. C.; Lodge, T. P. *Polymer Chemistry*, 2nd ed.; CRC Press, Taylor & Francis Group: Boca Raton, FL, 2007; pp 225−230.
37. Helfand, E.; Sapse, A. M. Theory of Unsymmetric Polymer−Polymer Interfaces. *J. Chem. Phys.* **1975**, *62*, 1327–1331.
38. Hong, S. W.; Gu, W.; Huh, J.; Sveinbjornsson, B. R.; Jeong, G.; Grubbs, R. H.; Russell, T. P. On the Self-Assembly of Brush Block Copolymers in Thin Films. *ACS Nano* **2013**, *7*, 9684–9692.
39. Hillmyer, M. A.; Bates, F. S. Synthesis and Characterization of Model Polyalkane-Poly(Ethylene Oxide) Block Copolymers. *Macromolecules* **1996**, *29*, 6994–7002.
40. Dalsin, S. J.; Hillmyer, M. A.; Bates, F. S. Linear Rheology of Polyolefin-Based Bottlebrush Polymers. *Macromolecules* **2015**, *48*, 4680–4691.
41. Matsen, M.; Schick, M. Stable and Unstable Phases of a Diblock Copolymer Melt. *Phys. Rev. Lett.* **1994**, *72*, 2660–2663.
42. Matsen, M. W. Melts of Semiflexible Diblock Copolymer. *J. Chem. Phys.* **1996**, *104*, 7758–7764.
43. Matsen, M. W. Fast and Accurate SCFT Calculations for Periodic Block-Copolymer Morphologies Using the Spectral Method with Anderson Mixing. *Eur. Phys. J. E: Soft Matter Biol. Phys.* **2009**, *30*, 361–369.